

Measurement of the muon anomalous precession frequency ω_a in the Fermilab Muon $g - 2$ Experiment

Sean B. Foster^{a,b,*}

^aon behalf of the Muon $g-2$ Collaboration[†]

^bDepartment of Physics and Astronomy, University of Kentucky, Lexington, Kentucky, 40506, USA

E-mail: sean.foster@uky.edu

The Fermilab Muon $g - 2$ Experiment was designed to measure the muon's anomalous magnetic moment $a_\mu = (g - 2)/2$ to 140 parts per billion. The value of a_μ is proportional to the difference frequency $\omega_a = \omega_s - \omega_c$ between the muon's cyclotron frequency and spin precession frequency in the uniform magnetic field of the $g - 2$ storage ring. The frequency ω_a is extracted from the time distribution of the mu-decay positrons recorded by 24 electromagnetic calorimeters positioned around the inner circumference of the storage ring. We will discuss the various approaches to the frequency determination including the reconstruction, fitting of time distributions, and procedures for handling the effects of gain changes, positron pileup and beam dynamics. We also discuss the data consistency checks and the strategy for the averaging of ω_a across the different analyses.

*The European Physical Society Conference on High Energy Physics (EPS-HEP2023)
21-25 August 2023
Hamburg, Germany*

*Speaker

[†]<https://muon-g-2.fnal.gov/collaboration.html>

1. Introduction

The Standard Model (SM) is the best tested theory of the fundamental particles and interactions of our universe. Despite its numerous successes in predicting fundamental physical quantities, the theory is incomplete: it does not account for such things as the matter/antimatter asymmetry in the universe or dark matter. One approach to probe the breakdown of the SM is to put it to stringent tests in which precise measurements and theoretical predictions are compared. A discrepancy would indicate the SM's incompleteness and could point towards new physics.

In recent years, an exciting precision test has involved the magnetic properties of the muon through the measurement and prediction of the muon's magnetic anomaly, denoted a_μ and defined as the fractional deviation of the muon's g -factor from 2¹: $a_\mu = (g - 2)/2$. Measuring a_μ has a long history, dating back to the 1960's [2]. The Muon $g - 2$ Experiment at Fermilab is the latest experiment and has the goal of measuring a_μ to a precision of 140 parts per billion (ppb) [5], a factor of four improvement over the previous measurement from Brookhaven [6].

The Muon $g - 2$ Collaboration released its first result in April 2021 [3]: the measurement achieved a precision of 460 ppb, comparable to the Brookhaven result, and the experimental world average pushed the tension with the SM prediction [7] to 4.2σ . This result was based on Run-1 data from 2018, which accounts for just 6% of the expected data for the experiment. The result's uncertainty was dominated by its statistical uncertainty.

On August 10, 2023, the Muon $g - 2$ Collaboration announced its second measurement of a_μ [4], reaching an unprecedented precision of 215 ppb, more than a factor of two better than its first result. The result is in agreement with both the Run-1 result and the Brookhaven result. This new measurement was based on Run-2/3 data, a dataset 4.7 times larger than Run-1, collected in 2019 and 2020. Through the additional data and improved methods, both the statistical and systematic uncertainties reduced by a factor 2.2. The experimental world average (combining the Brookhaven and the two Fermilab results) is now $a_\mu(\text{exp}) = 116\,592\,059(22) \times 10^{-11}$ [4].

The experimental technique used by the Muon $g-2$ Experiment consists in storing polarized positive muons in a storage ring magnet. The muons' spins precess in the magnetic field and, through precise measurements of both the magnetic field — which has been shimmed to extreme uniformity — and the precession frequency, the magnetic anomaly can be determined. In these proceedings, we describe the anomalous spin precession frequency measurement. Also at this conference are contributions describing the measurement of the uniform magnetic field [8], the determination of beam-dynamics corrections to the precession frequency [9], and an overview of the new result [10]. Refer to the overview for a status of the measurement and SM prediction comparison, which has become more complicated in the last couple years due to tensions in determining the hadronic vacuum polarization contributions to a_μ [7, 11–13].

2. The ω_a measurement

The Muon $g - 2$ Experiment at Fermilab uses a storage ring technique to measure a_μ . Polarized muons with a momentum of 3.1 GeV/c are produced by Fermilab's accelerator complex and injected

¹The contribution of 2 to the g -factor arises from the tree-level interaction between a muon and a photon and is also predicted by Dirac's theory of spin-1/2 fermions [1].

in 120 ns wide bunches into the 7.112 m radius storage ring with a uniform magnetic field of 1.451 T. In the presence of the magnetic field, a muon's spin precesses at the Larmor and Thomas precession frequency ω_s , while its momentum rotates at the cyclotron frequency ω_c . The difference between these two frequencies, $\omega_a = \omega_s - \omega_c$, is called the anomalous precession frequency and is proportional to both a_μ and the uniform magnetic field. As such, a measurement of the magnetic field and ω_a can be used to determine the magnetic anomaly.

The anomalous precession frequency is extracted from the time-modulation of the muon-decay positron's energy spectrum. In particular, the number of highest-energy positrons oscillates at ω_a due to the parity violation of the weak decay of the muon. The time-dependent energy spectrum is determined using a suite of 24 electromagnetic calorimeters [14] placed on the inner circumference of the storage ring, which intercepts the inwards-spiraling decay positrons. Each calorimeter is composed of a 6×9 grid of PbF_2 crystals, measuring $2.5 \times 2.5 \times 14 \text{ cm}^3$. When a decay positron passes through a crystal, it produces Cherenkov light, which is collected by a silicon photo-multiplier coupled to the back of the crystal. The signal is digitized and activity above a configurable threshold is isolated into time-islands containing raw traces for the subset of crystals adjacent to and including the above-threshold crystal. The raw traces are fit with empirically-determined template functions to extract the deposited energy and the positron arrival time. Two fit approaches are taken: a *local* approach, in which each crystal is fit individually, and a *global* approach, in which all crystals are fit simultaneously with a shared arrival time. In addition to these “event-based” approaches that reconstruct each and every positron, an “energy-integrated” method is also used in which a running calorimeter energy sum is stored. This method is statistically inferior than the event-based methods, but uses a completely separate raw data input, so provides a useful cross-check.

From the positron's arrival time and deposited energy, a time histogram over the $650 \mu\text{s}$ measurement period, corresponding to 10 lifetimes of the 3.1 GeV/c muons, can be filled. Filling the time histogram requires collapsing the energy information. A standard approach is to apply a flat energy threshold that only includes positrons above the threshold; the optimal threshold — the one that yields the smallest statistical uncertainty — is $\sim 1700 \text{ MeV}$. A more sophisticated approach

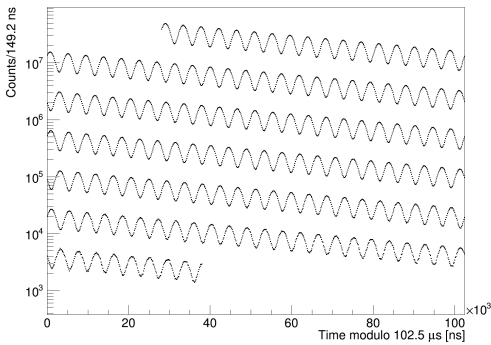


Figure 1: Time histogram for Run-3a data: number of asymmetry-weighted positrons from muon decay vs. time since muon injection. The data in this histogram account for about 50% of the total Run-2/3 data. The prominent oscillation is the ω_a signal.

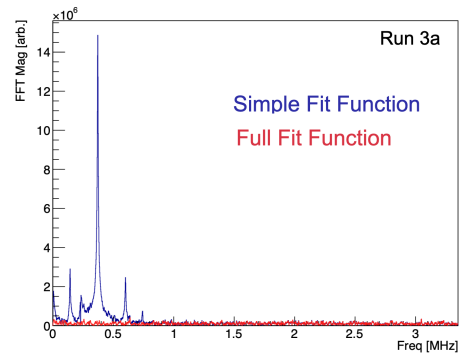


Figure 2: Fast Fourier transform of the Run-3a fit residuals using a simple fit model in blue (muon decay and $g - 2$ oscillation only) and the full model in red (see text). The peaks in the simple fit — due to unaccounted for beam frequencies — are removed in the full fit.

is to weight the positron counts by an energy-dependent function; the optimal weighting scheme uses the energy-dependent amplitude of the ω_a oscillation, called the asymmetry. An example time histogram from Run-3a, a subset of Run-3 which includes about 50% of the total decay positrons for the Run-2/3 data, can be found in Figure 1.

The ω_a frequency is determined through a χ^2 minimization calculated with a physically motivated fit model that accounts for the exponential muon decay, the $g - 2$ oscillation, beam oscillations that couple to detector acceptance, and muons lost before decay. The most important beam-dynamic frequency present in the data is due to the radial motion of the beam and is known as the coherent betatron oscillation (CBO). Detector gain is monitored with a state-of-the-art laser calibration system that allows for an empirical determination of gain changing effects [15]. Positron pileup, in which two or more positrons are misidentified as a single positron, is accounted for empirically, using the data itself to estimate and correct for pileup contamination. Accounting for all of these effects gives fits of good quality for the Run-2/3 data with reduced χ^2 's consistent with unity and featureless Fourier transforms of the fit residuals, as shown in Figure 2.

In addition to fits of good quality, various consistency checks were also performed. These checks included fitting each of the 24 calorimeters individually, fitting by energy bin, and grouping the data by external parameters such as ring temperature, magnet current, and day/night. Across all tested groupings, the extracted frequency was found to be consistent. Another particularly useful check is a fit start time scan, which is a robust test against “early-to-late” effects that induce a change in the $g - 2$ oscillation’s phase over the measurement period: a time-dependent phase is indistinguishable from a frequency bias. Fit start time scans revealed a stable extracted frequency.

In order to guard against mistakes and encourage the development of varied analysis approaches, the extraction of ω_a was performed by seven independent groups. Some groups, in addition to performing threshold and asymmetry-weighted analyses, also performed a ratio method analysis, which divides out slowly varying effects, thereby reducing sensitivity to early-to-late effects. New to the Run-2/3 analysis is the implementation of the asymmetry-weighted ratio method.

To avoid accidental bias, the analyses were performed with two levels of blinding: a common hardware blind that shifted the digitization clock frequency, and a software blind that shifted each analysis group’s frequency with respect to each other. To determine a single precession frequency, we performed a combination of the statistically optimal asymmetry-weighted analyses, of which there were six. Correlations between analysis methods and groups were estimated and incorporated into the averaging used to determine the final frequency and systematic uncertainties.

3. Run-2/3 improvements

The Run-2/3 precession frequency measurement benefits from improvements to both the statistical² and systematic uncertainties. The statistical uncertainty benefit is straightforward: the number of analyzed positrons in the Run-2/3 analysis is 4.7 times more than was analyzed in the Run-1 analysis, and the Run-1 analysis was statistically limited. The increased number of detected decay positrons resulted in a statistical uncertainty reduction from 460 ppb to 201 ppb.

Systematic uncertainties in the precession frequency measurement arise from effects that can cause a frequency bias, so-called early-to-late effects. These can arise from things like not properly

²The precession frequency measurement is the only part of the a_μ measurement with a statistical uncertainty.

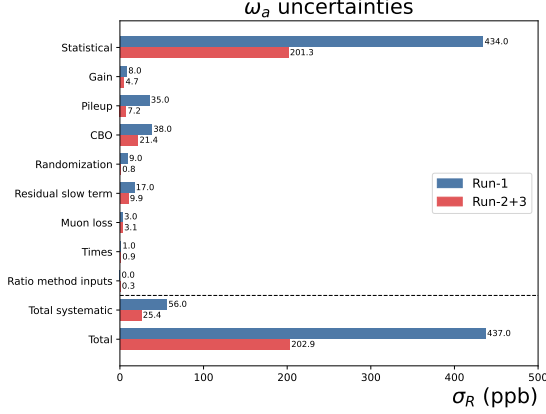


Figure 3: Uncertainties in the anomalous precession frequency measurement by category, comparing Run-1 (blue) to Run-2/3 (red). The Run-2/3 uncertainty is reduced by a factor of 2.2 compared to Run-1 due to improvements to both the statistical and systematic uncertainties.

correcting for pileup or a changing gain or for mismodeling the beam-dynamics effects like the CBO signal. For all possible sources, uncertainty estimations were performed. Figure 3 summarizes the size of the estimated systematic uncertainties by each of the identified categories and compares the estimates to Run-1. In Run-1, the dominant systematic uncertainties were from modeling the CBO and correcting for pileup. For the Run-2/3 analysis, significant effort was directed towards reducing these uncertainties, as we now describe.

The uncertainty due to pileup was 35 ppb in Run-1 and was largely due to the size of the pileup contamination that needed to be corrected. For the Run-2/3 analysis, a new clustering technique³, which leveraged the energy-dependence of the time resolution, was implemented and reduced the pileup contamination by a factor of four. In addition, more robust pileup subtraction techniques — which overlaid raw traces to produce constructed pileup events — were implemented and adopted by many analysis groups. These improvements reduced the uncertainty due to pileup to 7 ppb.

The Run-1 analysis was affected by an uncorrected residual slow effect whose physical origin was unknown. Modeling the effect as a possible gain or acceptance variation led to a 17 ppb uncertainty. Studies since then have revealed the physical origin of about 70% of the effect, which was due to using dual thresholds for identifying primary and secondary pulses on a digitized trace. Evidence of a smaller residual slow effect remains, but the uncertainty has been reduced to 10 ppb.

The dominant ω_a systematic uncertainty in Run-1 was due to modeling the CBO and it remains the dominant uncertainty in Run-2/3. The main source of uncertainty comes from modeling the decoherence envelope of the CBO signal and the time dependence of the CBO frequency. The additional data in Run-2/3 allowed testing more models and more stable running conditions⁴ resulted in a lower uncertainty of 21 ppb, compared to 38 ppb in Run-1. Taken all together, the total

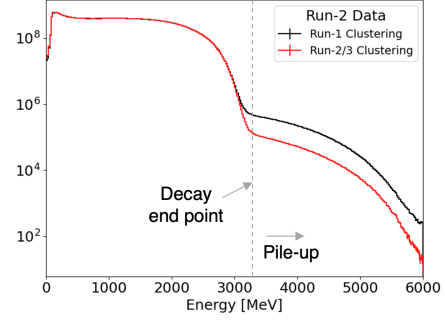


Figure 4: The decay positron energy spectrum using the Run-1 style clustering (blue) and the improved Run-2/3 style clustering (red). The high energy tail, which contains pileup-only events, shows that the level of pileup has been reduced by a factor of four.

³Clustering is the process by which crystal hits are groups together to form a reconstructed positron.

⁴In Run-1, broken electrostatic quadrupole resistors lead to a slow variation in the beam over the measurement period. For Run-2/3, the resistors were redesigned and replaced.

systematic uncertainty on ω_a has reduced from 56 ppb to 25 ppb.

4. Conclusions & outlook

The Muon $g - 2$ Collaboration has measured the muon magnetic anomaly to an unprecedented precision of 215 ppb, an improvement of more than a factor of two compared to our first result from 2021. The new measurement is in agreement with both our first result and the result from the Brookhaven experiment. The anomalous spin precession frequency measurement presented in these proceedings benefits from both the increased data and improved analysis techniques, leading to reductions in both the statistical and systematic uncertainties. The SM theory landscape has become complicated in the past couple years, making a comparison between experiment and theory difficult (see Reference [10] for a discussion). Looking ahead, the Muon $g - 2$ Collaboration has collected three additional years of data, having surpassed its design goal of 21 times the Brookhaven experiment [5]. In addition, improved running conditions through the implementation of a RF signal [17] to the focusing electrostatic quadrupole system [16] reduces the CBO oscillation. With more data and improved running conditions, we are on target to reach and improve upon our uncertainty goal.

Acknowledgements

We acknowledge support from the Fermi Research Alliance, LLC under Contract No. DE-AC02-07CH11359 with the U.S. DOE-OHEP. The author is supported by the US Department of Energy Grant DE-SC0013895 and U.S. National Science Foundation Award No. 2110479.

References

- [1] Paul A. M. Dirac, Proc. R. Soc. Lond. **A117**, 610–624 (1928).
- [2] R. L. Garwin, D. P. Hutchinson, S. Penman and G. Shapiro, Phys. Rev. **118**, 271 (1960).
- [3] B. Abi *et al.* (Muon $g - 2$ Collaboration), Phys. Rev. Lett. **126**, 141801 (2021).
- [4] D. Aguillard *et al.* (Muon $g - 2$ Collaboration), Phys. Rev. Lett. **131**, 161802 (2023).
- [5] J. Grange *et al.*, arXiv:1501.06858 (2016).
- [6] G. W. Bennett *et al.* (Muon $g - 2$ Collaboration), Phys. Rev. D **73**, 072003 (2006).
- [7] T. Aoyama *et al.*, Physics Reports **887**, 1-166 (2020).
- [8] S. Charity (on behalf of the Muon $g - 2$ Collaboration), EPS-HEP2023, 601 (2023).
- [9] O. Kim (on behalf of the Muon $g - 2$ Collaboration), EPS-HEP2023, 603 (2023).
- [10] G. Venanzoni (on behalf of the Muon $g - 2$ Collaboration), EPS-HEP2023, 837 (2023).
- [11] Sz. Borsanyi *et al.*, Nature **593**, 51 (2021).
- [12] M.N. Achasov *et al.* (SND collaboration), J. High Energ. Phys. **113** (2021).
- [13] F. V. Ignatov *et al.* (CMD-3 Collaboration), arXiv:2302.08834 (2023).
- [14] K. S. Khaw *et al.*, Nucl. Instrum. Methods Phys. Res., Sect. A **945**, 162558 (2019).
- [15] A. Anastasi *et al.* JINST **14**, P11025 (2019).
- [16] Y. K. Semertzidis *et al.*, Nucl. Instrum. Methods Phys. Res., Sect. A **503**, 458 (2003).
- [17] O. Kim *et al.*, New J. Phys. **22**, 063002 (2020).